Greater Than 20% Radiant Heat Conversion Efficiency of a Thermophotovoltaic Radiator/Module System Using Reflective Spectral Control

Bernard Wernsman, Richard R. Siergiej, Samuel D. Link, Robert G. Mahorter, Marc N. Palmisiano, Rebecca J. Wehrer, Robert W. Schultz, Gregory P. Schmuck, Rowan L. Messham, Susan Murray, Christopher S. Murray, Fred Newman, Daniel Taylor, David M. DePoy, and Thomas Rahmlow

***Abstract*—An InGaAs monolithic interconnected module (MIM) using reflective spectral control has been fabricated and measured in a thermophotovoltaic radiator/module system (radiator, optical cavity, and thermophotovoltaic module). Results showed that at a radiator and module temperature of 1039 °C and 25 °C, respectively, 23.6% thermophotovoltaic radiator/module system radiant heat conversion efficiency and 0.79 $\mathrm{W/cm^2}$ maximum thermophotovoltaic radiator/module system power density were obtained. The use of reflective spectral control increased the spectral efficiency and thus the thermophotovoltaic radiator/module system radiant heat conversion efficiency by $\sim$ 16% (relative). However, the amount of useful radiation reaching the MIM decreased by $\sim$ 7% (relative) compared to using transmissive spectral control. Also, the thermophotovoltaic system radiant heat conversion efficiency and maximum power density using either transmissive or reflective spectral control decreased as the MIM temperature increased. The MIM using reflective spectral control was found to be more sensitive to changes in the MIM temperature than the MIM using transmissive spectral control.**

***Index Terms*—InGaAs, photovoltaic cells, spectral control, thermophotovoltaic (TPV) cells.**

I. Introduction

Thermophotovoltaic (TPV) systems are similar to photovoltaic (PV) systems where an array of semiconductor devices is used to convert photons into electrical power. However, unlike a PV system that uses a constant light source (sun), the TPV system uses a hot radiator placed near the semiconductor array [1]. As a result, the photon spectrum and intensity that is converted to electrical power is different for the two systems. For PV, the solar spectrum has low intensity (100s of $\mathrm{mW/cm^2}$) with blackbody emission at ~ 5800 °C [2] while TPV converts a high intensity (10s of $\mathrm{W/cm^2}$) lower temperature spectrum with blackbody emission at < 1300 °C [1]. Since this lower temperature shifts the emitted light toward the infrared, the bandgap of the semiconductor material used to make TPV devices needs to be lower than that used for PV devices to obtain significant power density and efficiency in TPV systems.

For the last decade, TPV research has focussed on the use of direct bandgap III–V semiconductor materials ($\mathrm{In_xGa_{1-x}As_ySb_{1-y}}$) with bandgaps between 0.50 and 0.74 eV [3]–[5]. Two commercially available binary material substrates (InP and GaSb) are used for epitaxial growth of this TPV material. Along with having different lattice parameters (~ 6.10 and ~ 5.88 Å for GaSb and InP, respectively) [6] and bandgaps (~ 0.73 and ~ 1.38 eV for GaSb and InP, respectively) [6], the major distinction between these substrates is that GaSb is intrinsically p-doped and conductive [6] while InP can be made semi-insulating via Fe doping [7]. Thus, depending on the type of substrate used, single-junction diodes [8] (conductive substrate) and single-junction monolithic interconnected modules (MIMs) [9], [10] (semi-insulating substrate) can be readily made. MIMs using conductive substrates can be made via a wafer bonding/substrate removal technique [10], [11]. However, to date, no large area (≥ 4 $\mathrm{cm^2}$) MIMs have been successfully demonstrated using this method. An advantage of single-junction MIMs compared to single-junction diodes is that by monolithically series connecting many small diodes (MIM) the module output current for the same system operating conditions is lower, reducing its intrinsic I^2R losses and increasing its output power density and efficiency. Another advantage of the InP substrate is that it has insignificant free carrier absorption (extinction coefficient $(k) \leq 1 \times 10^{-5}$ for $1\ \mu\mathrm{m} \leq \mathrm{wavelength}(\lambda) \leq 10\ \mu\mathrm{m}$ [12]) allowing for increased photon recycling resulting in lower reverse saturation current densities and thus higher power densities and efficiencies [13]–[15]. Therefore, to create highly efficient and power dense MIM TPV devices grown on InP, InGaAs is used since this ternary has the lowest bandgap possible in the $\mathrm{In_xGa_{1-x}As_ySb_{1-y}}$ ($y = 1$) material system [6].

Although the bandgap of the TPV material is low, a large portion of the photon spectrum incident upon the TPV device does not have enough energy to produce electron-hole pairs that are used to create useful output power. To have a highly efficient TPV radiator/module system (radiator, optical cavity, and TPV MIM), nonradiative absorption of these relatively low-energy photons in the TPV MIM needs to be minimized through spectral control. Three types of spectral control methods can be employed [16].

The first eliminates the creation of the low-energy photons by reducing the long-wavelength emissivity of the radiator. This spectral control scheme can be created by either using a selective radiator [17] or a filtered radiator [18]. However, these schemes tend to also lower the emission of photons with enough energy to create electron-hole pairs, reducing the output power density of the TPV radiator/module system.

The second spectral control method is to reflect the relatively low-energy photons back toward the radiator (reflective spectral control), precluding these photons from entering the TPV device. This spectral control scheme can be created using a filter placed onto the front of the TPV device [19]. However, like the first spectral control scheme, this approach also tends to lower the amount of relatively high-energy photons reaching the TPV device, lowering the output power density of the TPV radiator/module system. It is important to note that reflective spectral control does not reduce the amount of high energy photons entering the device as much as the first spectral control method from above.

The third spectral control method allows most of the emitted photons to enter the TPV device (transmissive spectral control) but only the high-energy photons are absorbed while the low-energy photons are reflected back toward the radiator. The implementation of this spectral control strategy requires that a semi-insulating InP substrate with low free carrier absorption be used as discussed above. Also, a highly specular and reflective surface (like Au) must be placed onto the back of the wafer (back surface optical reflector), and the free carrier absorption of the material used to create the TPV device needs to be minimized [9], [10]. The advantage of this spectral control strategy is that the power density of the TPV radiator/module system can be maximized since

Manuscript received August 26, 2003; revised November 20, 2003. The review of this paper was arranged by Editor P. Panayotatos.

B. Wernsman, R. R. Siergiej, S. D. Link, R. G. Mahorter, M. N. Palmisiano, R. J. Wehrer, R. W. Schultz, G. P. Schmuck, and R. L. Messham are with Bechtel Bettis, Inc., West Mifflin, PA 15122 USA.

S. Murray, C. S. Murray, and F. Newman are with EMCORE Photovoltaics, Albuquerque, NM 87123 USA.

D. Taylor is with Bandwidth Semiconductor, LLC, Hudson, NH 03051 USA.

D. M. DePoy is with Lockheed Martin, Schenectady, NY 12301 USA.

T. Rahmlow is with Rugate Technologies, Inc., Oxford, CT 06804 USA.

Digital Object Identifier 10.1109/TED.2003.823247

TABLE I
MEASURED TPV RADIATOR/MODULE SYSTEM (RADIATOR, OPTICAL CAVITY, AND TPV MIM) PERFORMANCE USING A FILTERED AND UNFILTERED MIM

TPV Radiator/Module System Conditions			TPV System Performance					
Module	$T_{Radiator}$ (°C)	T_{MIM} (°C)	I_{SC} (A)	V_{OC} (V)	FF	PD_{max} (W/cm^2)	Q_{abs} (W)	η_{RH} (%)
Unfiltered MIM [21]	887	26	0.190	11.9	0.677	0.383	9.27	16.5
	955	26	0.268	12.1	0.674	0.548	11.8	18.6
	956	38	0.276	11.7	0.661	0.535	11.8	18.1
	956	46	0.281	11.4	0.654	0.520	12.1	17.3
	956	54	0.287	11.1	0.639	0.508	12.0	16.9
	956	65	0.292	10.7	0.617	0.480	12.1	15.9
	1027	27	0.381	12.3	0.672	0.788	15.4	20.5
	1058	27	0.440	12.4	0.660	0.900	17.5	20.6
Filtered MIM	871	24	0.151	11.9	0.664	0.297	6.11	19.4
	927	24	0.212	12.1	0.674	0.432	8.01	21.6
	955	24	0.247	12.2	0.676	0.509	9.15	22.3
	955	38	0.250	11.8	0.657	0.482	9.18	21.0
	954	46	0.250	11.4	0.650	0.463	9.13	20.3
	955	52	0.252	11.3	0.643	0.456	9.10	20.0
	953	64	0.251	10.8	0.624	0.421	8.99	18.7
	983	25	0.288	12.3	0.674	0.597	10.4	23.0
	1039	25	0.382	12.5	0.662	0.790	13.4	23.6

Nomenclature:
T_{Radiator} : Radiator Temperature
T_{MIM} : MIM or Filtered MIM Temperature
$\mathrm{I_{SC}}$: Short Circuit Current
$\mathrm{V_{OC}}$: Open Circuit Voltage
FF : Fill Factor
$PD_{\max}$: Maximum System (Radiator, Optical Cavity, and TPV MIM) Output Power Density
$\mathrm{Q_{abs}}$: Heat Absorbed
η_{RH} : Radiator/Module System (Radiator, Optical Cavity, and TPV MIM) Radiant Heat Transfer Efficiency

more photons are allowed into the device using this spectral control scheme than by using the other two methods from above. Furthermore, any combination of these three spectral control strategies can be used together to enhance the efficiency of the TPV radiator/module system.

The best performing TPV radiator/module system operating at a temperature of 1058 °C reported to date produced 0.90 W/cm^2 at a radiant heat transfer efficiency [20] of 20.6% [21]. This system used a 5.4 × 5.4 cm^2 etched SiC graybody radiator placed $\sim$ 2 mm away from a 2 × 2 cm^2 MIM operating at a temperature of $\sim$ 26 °C in a vacuum (see [20] for schematic). The MIM was made using 30 series connected 0.6 eV InGaAs/InPAs double heterostructure diodes employing an n/p/n tunnel-junction architecture to minimize the series resistance [9], [10]. Since this device used transmissive spectral control, a Si_3N_4 layer was used on the front of the device as both the interconnect dielectric and anti-reflective coating, while a specular Si_3N_4/Au coating was placed onto the polished back of the InP substrate as the back surface reflector. An InPAs buffer region was used to change the lattice parameter from that of InP to that of 0.6-eV InGaAs [22]. This buffer region was n-doped and used as the lateral conduction layer (LCL). Since the bandgap of the InPAs buffer/LCL is much larger than 0.6 eV, parasitic absorption of photons was minimized. The low reverse saturation current density of 0.39 μA/cm^2 for this MIM indicates that the material grown above the buffer region was lattice-matched to the top of the buffer region with an apparent defect density of $\leq 1 \times 10^6$ cm^{-2}. The MIM was fabricated using standard photolithographic techniques and wet chemistry [23]. The high radiant heat conversion efficiency and power density of the TPV system using this MIM indicate that the processing introduced no other major defects to the device.

II. EXPERIMENTAL PROCEDURE AND RESULTS

Although the radiant heat transfer efficiency of the radiator/module system from above was large, the efficiency of the transmissive spectral control [14] was only $\sim$ 60%, making the efficiency of the 0.6 eV n/p/n InGaAs diode $\sim$ 34%. Placing a front surface filter with a spectral control efficiency $>$ 60% onto the device (reflective spectral control) would increase the system radiant heat transfer efficiency. The following shows the results obtained when reflective spectral control was added.

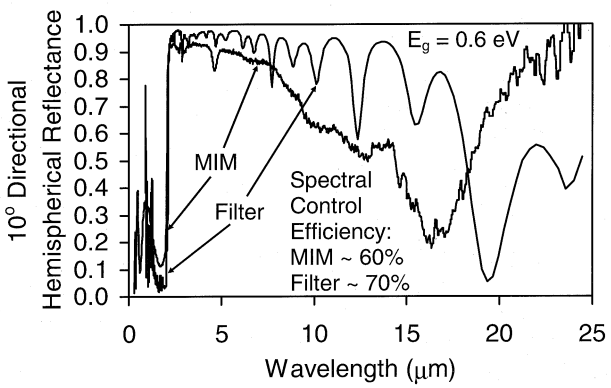

Fig. 1. The 10° directional hemispherical reflectance of MIM and filter showing increased spectral control efficiency with the use of a filter.

The front surface filter, glued onto the MIM using Tra-Con Bipax Tra-Bond BA-2115 optical epoxy, was a multilayer Sb_2Se_3/YF_3 dielectric stack grown on a highly n-doped InPAs plasma filter. On the back of this filter, a multilayer Sb_2Se_3/YF_3 antireflective coating was also grown. The measured 10° directional hemispherical reflectance of this filter and the MIM is given in Fig. 1. As shown, the spectral control efficiency [14] of the filter was $\sim$ 70%. This efficiency was 10% (absolute) higher than that for the MIM since the reflectance of the low energy photons ($\lambda >\sim 2$ μm) was larger for the filter compared to the

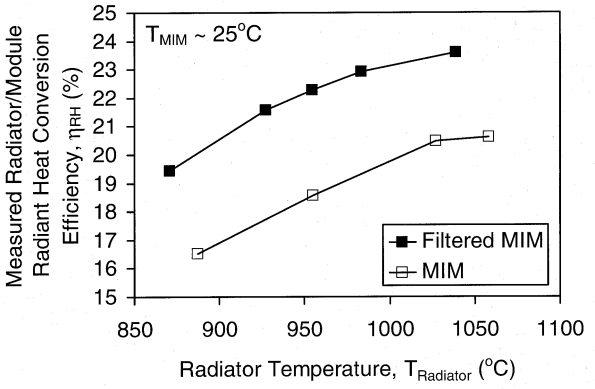

Fig. 2. Measured radiator/module system radiant heat conversion efficiency of the filtered and unfiltered MIM cases at a MIM temperature ($T_{\rm MIM}$) of $\sim$ **25** °C as a function of radiator temperature ($T_{\rm Radiator}$) showing that the radiator/module system using the filtered MIM is more efficient.

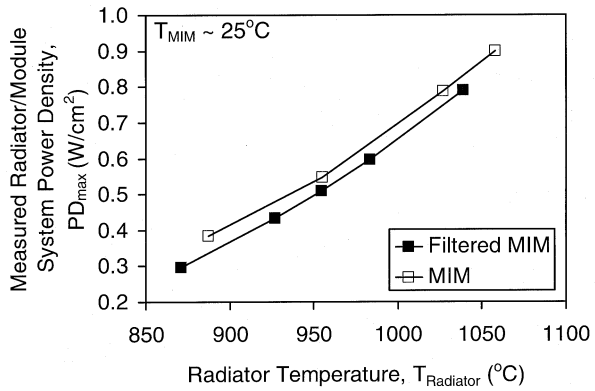

Fig. 3. Measured radiator/module system maximum power density of the filtered and unfiltered MIM cases at a MIM temperature ($T_{\rm MIM}$) of $\sim$ **25** °C as a function of radiator temperature ($T_{\rm Radiator}$) showing that the radiator/module system using the unfiltered MIM is more power dense.

MIM. The angle of incidence weighted reflectance was used to calculate the spectral control efficiencies as described in [14]. Although the reflectance of the filter was lower than that of the MIM for the relatively high energy photons, the amount of light allowed into the MIM diodes was $\sim 84\%$ while it was only $\sim 78\%$ for the filtered MIM due to extra absorption in the filter and to an index mismatch between the filter/glue and the Si_3N_4 antireflective coating on the MIM.

Testing of the filtered MIM occurred in the experimental setup previously described [20]. The measured results from this setup using the unfiltered and filtered MIM are given in Table I. As shown in Fig. 2 and Table I for a MIM temperature ($T_{\rm MIM}$) of ~ 25 °C, the radiator/module system radiant heat transfer efficiency ($\eta_{\rm RH}$) [20] for the filtered MIM case was larger than that for the MIM alone. For example, at a radiator temperature ($T_{\rm Radiator}$) of ~ 955 °C, $\eta_{\rm RH}$ increased from 18.6% to 22.3% (16% relative increase) with the addition of the filter. The maximum measured $\eta_{\rm RH}$ was 23.6% at $T_{\rm Radiator} = 1039$ °C. However, as shown in Fig. 3 and Table I for $T_{\rm MIM} \sim 25$ °C, the radiator/module system maximum power density ($PD_{\rm max}$) for the filtered MIM was lower than that for the MIM alone. For example, at $T_{\rm Radiator}$ of ~ 955 °C, the maximum measured $PD_{\rm max}$ decreased from 0.548 W/cm^2 to 0.509 W/cm^2 ($\sim 7\%$ relative decrease) when using the filter due to the lower amount of light allowed into the MIM. Even with this decrease in $PD_{\rm max}$ for the filtered case, 0.790 W/cm^2 was measured at a $T_{\rm Radiator}$ of 1039 °C.

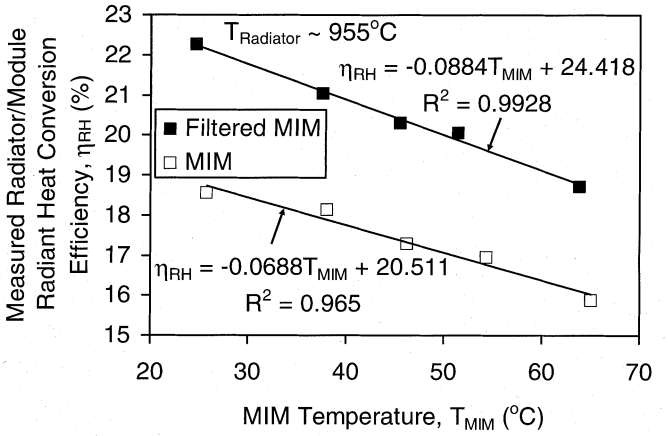

Fig. 4. Measured radiator/module system radiant heat conversion efficiency of the filtered and unfiltered MIM cases at a radiator temperature ($T_{\rm Radiator}$) of $\sim$ **955** °C as a function of MIM temperature ($T_{\rm MIM}$) showing that the negative temperature coefficient for the radiator/module system using the filtered MIM is larger than that for the unfiltered MIM.

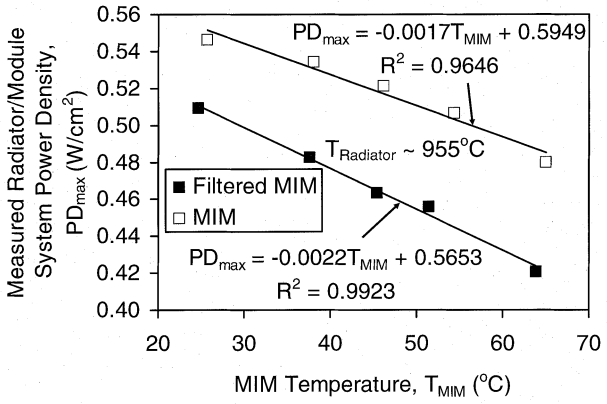

Fig. 5. Measured radiator/module system maximum power density of the filtered and unfiltered MIM cases at a radiator temperature ($T_{\rm Radiator}$) of $\sim$ 955 °C as a function of MIM temperature ($T_{\rm MIM}$) showing that the negative temperature coefficient for the radiator/module system using the filtered MIM is larger than that for the unfiltered MIM.

Some TPV applications require that the TPV module temperature be higher than 25 °C [24]. Figs. 4 and 5 show the effect of $T_{\rm MIM}$ on the radiator/module system performance. As shown in Figs. 4 and 5, $\eta_{\rm RH}$ and $PD_{\rm max}$ decreased as $T_{\rm MIM}$ increased for both the filtered and unfiltered case where $\eta_{\rm RH}$ and $PD_{\rm max}$ exhibit larger negative temperature coefficients for the filtered MIM case. This larger negative temperature coefficient for $\eta_{\rm RH}$ and $PD_{\rm max}$ may be due to the temperature dependence of the MIM bandgap [25] while the filter cutoff wavelength that was designed to operate at 25 °C is independent of temperature. Therefore, if a less sensitive temperature coefficient is desired at higher MIM temperature operation, the cutoff wavelength of the filter needs to match the MIM bandgap at the desired operating temperature.

III. Conclusion

An InGaAs MIM using reflective spectral control for TPV applications has been fabricated and measured. Results show that the use of reflective spectral control increased the spectral efficiency and thus the TPV radiator/module system radiant heat transfer efficiency by $\sim 16\%$ (relative) at the expense of reducing the amount of useful radiation reaching the MIM by $\sim 7\%$ (relative). At a radiator and MIM

temperature of 1039 and 25 °C, respectively, 23.6% radiator/module system (radiator, optical cavity, and TPV MIM) radiant heat transfer efficiency and 0.79 W/cm^2 maximum radiator/module system power density were measured while using reflective spectral control. The TPV radiator/module system radiant heat transfer efficiency and maximum power density using the MIM with either transmissive or reflective spectral control decreased as the MIM temperature increased. The MIM using reflective spectral control was found to be more sensitive to changes in the MIM temperature than the MIM using transmissive spectral control. This difference in temperature sensitivity for the MIM using reflective and transmissive spectral control may be due to the MIM bandgap changing with temperature and a filter cutoff wavelength that does not change with temperature. By designing the filter for the desired operating temperature, the MIM with reflective spectral control should have the same temperature sensitivity as the MIM using transmissive spectral control.

REFERENCES

[1] T. J. Coutts and M. C. Fitzgerald, "Thermophotovoltaics," *Sci. Amer.*, vol. 279, no. 3, pp. 90–95, 1998.

[2] *CRC Handbook of Chemistry and Physics*, 67th ed., R. C. Weast, M. J. Astle, and W. H. Beyer, Eds., CRC, Boca Raton, FL, 1986.

[3] S. Wojtczuk, E. Gagnon, L. Geoffroy, and T. Parados, "$In_xGa_{1-x}As$ thermophotovoltaic cell performance vs. bandgap," in *Proc. NREL Thermophotovoltaic Gen. Electricity Conf.*, vol. 321, AIP Conf. Proc., 1995, pp. 177–187.

[4] C. A. Wang, H. K. Choi, D. C. Oakley, and G. W. Charache, "Extending the cutoff wavelength of lattice-matched GaInAsSb/GaSb thermophotovoltaic devices," in *Proc. NREL Thermophotovoltaic Gen. Electricity Conf.*, vol. 460, AIP Conf. Proc., 1999, pp. 256–265.

[5] C. A. Wang, H. K. Choi, S. L. Ransom, G. W. Charache, L. R. Danielson, and D. M. DePoy, "High-quantum-efficiency 0.5 eV GaInAsSb/GaSb thermophotovoltaic devices," *Appl. Phys. Lett.*, vol. 75, pp. 1305–1307, 1999.

[6] P. S. Dutta, H. L. Baht, and V. Kumar, "The physics and technology of gallium antimonide: An emerging optoelectronic material," *J. Appl. Phys.*, vol. 81, pp. 5821–5870, 1997.

[7] F. X. Zach, "New insights into the compensation mechanism of Fe-doped InP," *J. Appl. Phys.*, vol. 75, pp. 7894–7903, 1994.

[8] Z. A. Shellenbarger, M. G. Mawk, J. A. Cox, M. I. Gottfried, P. E. Sims, J. D. Lesko, J. B. McNeely, L. C. DiNetta, and R. L. Mueller, "Improvements in GaSb-based thermophotovoltaic cells," in *Proc. NREL Thermophotovoltaic Gen. Electricity Conf.*, vol. 401, AIP Conf. Proc., 1997, pp. 117–128.

[9] D. M. Wilt, C. S. Murray, N. S. Fatemi, and V. Weizer, "n/p/n tunnel junction InGaAs monolithic interconnected module (MIM)," in *Proc. NREL Thermophotovoltaic Gen. Electricity Conf.*, vol. 460, AIP Conf. Proc., 1999, pp. 152–160.

[10] D. Wilt, R. Wehrer, M. Palmisiano, M. Wanlass, and C. Murray, "Monolithic interconnected modules (MIMs) for thermophotovoltaic energy conversion," *Semicond. Sci. Technol.*, vol. 18, pp. S209–S215, 2003.

[11] C. A. Wang, R. K. Huang, D. A. Shiau, M. K. Connors, P. G. Murphy, P. W. O'Brien, A. C. Anderson, D. M. DePoy, G. Nichols, and M. N. Palmisiano, "Monolithically series-interconnected GaInAsSb/AlGaAsSb/GaSb thermophotovoltaic devices with an internal backsurface reflector formed by wafer bonding," *Appl. Phys. Lett.*, vol. 83, pp. 1286–1288, 2003.

[12] E. D. Palik, *Handbook of Optical Constants of Solids*. San Diego, CA: Academic, 1985.

[13] C. H. Henry, "Limiting efficiencies of ideal single and multiple energy gap terrestrial solar cells," *J. Appl. Phys.*, vol. 51, pp. 4494–4500, 1980.

[14] P. F. Baldasaro, J. E. Raynolds, G. W. Charache, D. M. DePoy, C. T. Ballinger, T. Donovan, and J. M. Borrego, "Thermodynamic analysis of thermophotovoltaic efficiency and power density tradeoffs," *J. Appl. Phys.*, vol. 89, pp. 3319–3327, 2001.

[15] J. F. Beausang, "The Thermodynamics of Thermophotovoltaics," M.S. thesis, Renssalaer Polytech. Inst., Troy, NY, 2002.

[16] L. M. Fraas, J. E. Avery, H. X. Huang, and R. V. Martinelli, "Thermophotovoltaic system configurations and spectral control," *Semicond. Sci. Technol.*, vol. 18, pp. S165–S173, 2003.

[17] Z. Chen, P. L. Adiar, and M. F. Rose, "Multiple-dopant selective emitter," in *Proc. NREL Thermophotovoltaic Gen. Electricity Conf.*, vol. 401, AIP Conf. Proc., 1997, pp. 181–188.

[18] L. Fraas, J. Samaras, J. Avery, and L. Minkin, "Antireflection coated refractory metal matched emitters for use with GaSb thermophotovoltaic generators," in *Proc. IEEE Photovoltaics Specialists Conf.*, 2000, pp. 1020–1023.

[19] D. E. Pierce and G. Guazzoni, "High temperature optical properties of thermophotovoltaic emitter components," in *Proc. NREL Thermophotovoltaic Gen. Electricity Conf.*, vol. 460, AIP Conf. Proc., 1999, pp. 177–190.

[20] R. G. Mahorter, B. Wernsman, R. M. Thomas, and R. R. Siergiej, "Thermophotovoltaic system testing," *Semicond. Sci. Technol.*, vol. 18, pp. S232–S238, 2003.

[21] R. R. Siergiej, B. Wernsman, S. A. Derry, R. G. Mahorter, R. J. Wehrer, S. D. Link, M. N. Palmisiano, R. L. Messham, S. Murray, C. S. Murray, F. Newman, J. Hills, and D. Taylor, "20% efficient InGaAs/InPaS thermophotovoltaic cells," in *Proc. Thermophotovoltaic Gen. Electricity Conf.*, vol. 653, AIP Conf. Proc., 2003, pp. 414–423.

[22] S. L. Murray, F. D. Newman, C. S. Murray, D. M. Wilt, M. W. Wanlass, P. Ahrenkiel, R. Messham, and R. R. Siergiej, "MOCVD growth of lattice-matched and mismatched InGaAs materials for thermophotovoltaic energy conversion," *Semicond. Sci. Technol.*, vol. 18, pp. S202–S208, 2003.

[23] R. J. Wehrer, M. W. Wanlass, B. Wernsman, J. J. Carapella, S. P. Ahrenkiel, D. M. Wilt, and C. S. Murray, "0.74/0.55-eV $Ga_xIn_{1-x}As/\mathbf{InAs_yP_{1-y}}$ monolithic, tandem, MIM TPV converters: Design, growth, processing and performance," in *Proc. IEEE Photovoltaic Spec. Conf.*, 2002, ISBN: 0-7803-7472-X, pp. 884–887.

[24] A. Shock, C. Or, and V. Kumar, "Small radioisotope thermophotovoltaic (RTPV) generators," in *Proc. NREL . Thermophotovoltaic Gen. Electricity Conf.*, vol. 358, AIP Conf. Proc., 1996, pp. 81–97.

[25] J. I. Pankove, *Optical Processes in Semiconductors*. New York: Dover, 1975.